Theory of zeolite supralattices: Se in zeolite Linde type A

2001 J. Phys.: Condens. Matter 13 10433

(http://iopscience.iop.org/0953-8984/13/46/313)

INSTITUTE OF PHYSICS PUBLISHING JOURNAL OF PHYSICS: CONDENSED MATTER

J. Phys.: Condens. Matter **13** (2001) 10433–10457 PII: S0953-8984(01)23035-5

Theory of zeolite supralattices: Se in zeolite Linde type A

Alexander A Demkov[1] **and Otto F Sankey**[2]

[1] Physical Sciences Research Laboratories, Motorola Incorporated, Tempe, AZ 85284, USA
[2] Department of Physics and Astronomy, Arizona State University, Tempe, AZ 85287, USA

E-mail: alex.demkov@motorola.com

Received 16 March 2001
Published 2 November 2001
Online at stacks.iop.org/JPhysCM/13/10433

Abstract

We study theoretically properties of Se clusters in zeolites, and choose zeolite Linde type A (LTA) as a prototype system. The geometries of free-space Se clusters are first determined, and we report the energetics and electronic and vibrational properties of these clusters. The work on clusters includes an investigation of the energetics of C_3–C_1 defect formation in Se rings and chains. The electronic properties of two Se crystalline polymorphs, trigonal Se and α-monoclinic Se, are also determined. Electronic and vibrational properties of the zeolite LTA are investigated. Next we investigate the electronic and optical properties of ring-like Se clusters inside the large α-cages of LTA. We find that Se clusters inside cages of silaceous LTA have very little interaction with the zeolite, and that the HOMO–LUMO gaps (HOMO standing for highest occupied molecular orbital and LUMO for lowest unoccupied molecular orbital) are nearly those of the isolated cluster. The HOMO–LUMO gaps of Se_6, Se_8, and Se_{12} are found to be similar, which makes it difficult to identify them experimentally by absorption spectroscopy. We find that the zeolite/Se_8 nanocomposite is lower in energy than the two separated systems. We also investigate two types of infinite chain encapsulated in LTA. Finally, we carry out finite-temperature molecular dynamics simulations for an encapsulated Se_{12} cluster, which shows cluster melting and formation of nanoscale Se droplets in the α-cages of LTA.

(Some figures in this article are in colour only in the electronic version)

1. Introduction

A nanocomposite, or a combination of a host matrix and guest nanocluster, is an attractive concept from several points of view [1]. By using the large cages (or channels) of zeolites as pockets for storing semiconductor or metallic clusters, one can form artificial periodic

structures, termed 'supralattices'. Such systems often have novel magnetic, optical, or electronic properties. Zeolites have wide electronic band gaps which, in some cases, allow electronic states of the 'guest' cluster to exist largely unperturbed by the framework and to be optically or magnetically active [2]. A description of some of the theoretical methods for treating such complex systems, and example calculations, can be found in reference [3].

In this paper we investigate theoretically the electronic and vibrational modes of free Se clusters, and Se clusters in the cages of zeolite Linde type A (LTA). Selenium in zeolites has had a very long history, starting with the early work of Bogomolov *et al* [4]. Selenium can exhibit a variety of structures and this diversity is manifested in zeolites as well. In zeolite materials with channels such as mordenite, Se self-assembles into chain-like structures similar to that of trigonal Se. In zeolite A with cages, Se is incorporated as ring-like structures similar to those in monoclinic Se. Zeolite-encapsulated Se is photosensitive [5–7]. Visible light causes changes in the encapsulated clusters, which are probably structural in nature, and new absorption bands, Raman bands, and ESR signatures are found.

This paper is organized as follows. In section 2, we briefly describe the electronic structure-based quantum molecular dynamics (QMD) technique that we use to study these systems. In section 3, we first discuss selenium, and report the results of our calculations of free Se clusters, and finally our results for different bulk phases of crystalline Se. In section 4, we discuss the zeolite LTA, and report our results on Se rings encapsulated in the cages of LTA and on LTA loaded with Se chains. A comparison is made of our theoretical results with those from optical absorption experiments. The vibrational spectra are reported as well; these are relevant to Raman and infrared (IR) experiments. We conclude this section with a discussion of a high-temperature dynamical simulation of a large Se_{12} cluster in the α-cage of LTA, where we observe subsystem melting and evaporation; i.e. the cluster undergoes a phase transition but is surrounded by an intact crystalline LTA framework. Finally, in section 5 we give our conclusions.

2. Method

The theoretical method that we use is an electronic structure technique which employs the local density approximation and a minimal sp^3 basis of local orbitals. The electronic structure method Fireball96 [17] has full quantum molecular dynamics capabilities, which allows us to calculate total energies, forces, and the electronic structure, and allows the atoms to move in time in response to the forces. To optimize a structure, we allow the force to move the atoms as in a molecular dynamics algorithm, but add a fictitious velocity-dependent damping force to arrive at a final zero-force (energy-minimum) configuration. The method is based on density functional theory within the local density approximation (LDA), and the pseudopotential approximation. The Ceperley–Alder form of the exchange–correlation potential [18] is used. For selenium, silicon, and oxygen, we use the 'hard' norm-conserving pseudopotentials of the Hamann–Schlüter–Chiang [19] type. A simplified self-consistent energy functional [17] generalized from that due to Harris [20, 21] is employed in combination with the minimal basis of local 'Fireball' orbitals [21]. Forces acting on each atom are computed using a generalization of the Hellmann–Feynman theorem [21]. We have chosen the confinement 'Fireball' radii for the O, Si, and Se orbitals to be $r_c = 3.6$, 5.0, and 4.32 Bohr, respectively. We use Monkhorst–Pack special k-points to perform integrations over the Brillouin zone [22]. The method has been tested on a variety of systems and further examples are given in reference [23].

3. Selenium

Selenium was discovered in 1817 by J J Brezelies (who also discovered Si, Ge, and Th, and introduced the concept of catalysis) and J G Gahn (the discoverer of Mn), and given a name derived from a Greek word for the Moon. Even though it is highly toxic, Se has found many applications in photocells, xerography, rectifiers, colouring of glasses, and dehydration and catalysis in organic synthesis, and as a vulcanization agent for natural rubber.

Several allotropes of Se are known. The most stable form of Se at low temperature and pressure is grey or metallic selenium. It crystallizes in a trigonal structure and consists of helical chains. Its density of 4.82 g cm^{-3} is the highest density of all the Se allotropes. Another allotrope with chains is 'red' amorphous Se, but this allotrope has a much lower density of 4.26 g cm^{-3}, which is the lowest density among the Se allotropes. Vitreous or black Se is a cyclic polymer with rings containing up to 1000 atoms. It is non-conducting and has a density of 4.28 g cm^{-3}. In addition to red amorphous Se, there are two forms of red crystalline Se. Both α-monoclinic and β-monoclinic Se consist of Se_8 rings (four per unit cell), and they each have a density of 4.46 g cm^{-3}. Finally, a monoclinic form with six-membered rings has also been reported [24]. Thus in summary, Se forms two structure types—ring-based structures and chain-based structures. Se rings are stable and have been observed in the gas phase [25], while free Se chains are not stable. Interestingly, these two topologically quite different structures are remarkably similar on the local scale of a few interatomic distances.

In this paper, we investigate various Se clusters (rings and chains) in cavities and channels of zeolite LTA. We begin, however, with isolated Se clusters. Insight into the electronic and geometrical structure of small clusters and their aggregates is also of importance for an understanding of the amorphous phase of Se. Amorphous Se has been extensively studied; the most recent theoretical work was done by Hohl and Jones [26] and Zhang and Drabold [27]. After we discuss clusters, we next consider two crystalline Se polymorphs—the ring-based α-monoclinic structure and the chain-based grey Se structure. We then proceed with the discussion of the structure and electronic and vibrational properties of Se clusters and chains encapsulated in zeolite A.

3.1. Clusters

The molecular nature of Se solids—and the possible presence of molecular fragments in amorphous and liquid Se—makes a study of selenium clusters a required initial step towards an understanding of condensed phases. Se clusters have been recently studied experimentally by Becker *et al* [25]. Photoelectron spectroscopy performed using a molecular beam revealed the presence of Se_5, Se_6, Se_7, and Se_8 clusters and their aggregates. Becker *et al* reported that as the cluster size increases (Se_n clusters with n up to 25 were studied) the photoelectron spectra converge to that of the amorphous solid. Hohl *et al* [30] have studied theoretically selenium clusters Se_3 to Se_8 using density functional-based molecular dynamics, and have determined the ground-state geometries and ionization energies. The geometrical structures of Se_3, Se_4, Se_6, Se_7, and Se_8 are found to be very similar to their sulphur counterparts. No experimental data exist for Se_5, but a cyclic structure has been predicted for the ground state. In a later paper, Li *et al* [39] obtained theoretically findings similar to those of Hohl *et al*.

We now discuss our theoretical results for small Se clusters in free space. Specifically, we have studied Se_2, Se_3, Se_4, Se_5, Se_6, Se_7, Se_8, Se_{12}, and Se_{16} clusters. The bond lengths, HOMO–LUMO electronic gaps, and total energies per atom for these clusters are listed in table 1. Ball-and-stick models of many of these clusters are given in figures 1(a)–1(i). The total energies per atom in Se clusters are given (table 1) relative to those of an infinite Se chain.

Table 1. The total energies per atom, bond lengths, and HOMO–LUMO electronic gaps in Se clusters. The total energies are relative to that of an infinite optimized helical Se chain.

Cluster	Bond lengths	HOMO–LUMO gap (eV)	Energy/atom (eV)
Se_2	2.16	0.00	1.314
Se_3	2.19	1.10	0.707
Se_4	2.35	2.00	0.306
Se_5 (cyclic)	2.31–2.37	2.79	0.088
Se_5 (C3–C1)	2.35, 2.177	1.77	0.336
Se_6 (cyclic D_{3d})	2.32	3.60	0.016
Se_7 (cyclic)	2.34–2.76	3.31	0.008
Se_7 (C3–C1)	2.32, 2.19	2.22	0.149
Se_8 (cyclic D_{4d})	2.31	3.56	−0.022
Se_{12} (cyclic D_{3d})	2.31	3.58	−0.027
Se_{12} (cyclic)	2.28–2.38	2.60	0.001
Se_{12} (short chain)	2.31–2.41, 2.20	0.16	0.194
Se_{12} (long chain)	2.31–2.39, 2.20	0.00	0.221
Se_{16} (cyclic D_{4d})	2.31	3.28	−0.017
Se_{16} (cyclic D8R)	2.31	2.98	−0.013

We note that the large cyclic cluster, Se_8 (D_{4d}), Se_{12} (cyclic), Se_{16} (D_{4d}), and the Se_{16} double 8-ring (D8R) are lower in energy than a fully optimized isolated helical chain (the chain is pitched similarly to trigonal Se (t-Se) with a lattice constant of 9.85 Å). We now briefly discuss our findings for each of the clusters considered.

The Se dimer (Si_2) is found to have a bond length of 2.16 Å and this is comparable to the experimental value of 2.17 Å. There is no HOMO–LUMO gap due to an orbital degeneracy. The equilibrium structure of the Se_3 cluster (figure 1(a)) is an isosceles triangle with two equal Se–Se bond lengths of 2.19 Å, and an apex angle of 115°. This result is in good agreement with those given by Hohl *et al* [30]. We find a HOMO–LUMO gap of 1.1 eV, which is about a half of the value reported by Li *et al* [39]. The Se_4 cluster (figure 1(b)) is found to be a rhombus (although not quite flat) with an angle of 87° and a bond length of 2.35 Å. The HOMO–LUMO gap is 2.0 eV.

We have examined two Se_5 structures. The lowest-energy cyclic structure is shown in figure 1(c). The bond angles range from 93.3° to 102.4°, and the bond lengths are about 2.32 Å, with the exception of one bond length of 2.37 Å (a similar result was reported by Hohl *et al* [30]), and the torsion angle is 61.3°. The charge transfer between the Se atoms is very small ($|Q| \sim 0.02e$). We found another dynamically stable Se_5 structure (figure 1(d)), but it is 1.24 eV higher in energy than the cyclic structure. The bond lengths in the Se_4 fragment of the high-energy structure are very similar to that in the Se_4 cluster. The bond length between the one-coordinated (hereafter referred to as C_1) atom and the three-coordinated (C_3) atom is 2.177 Å, which is close to that of a dimer. The HOMO–LUMO gap of this structure is reduced compared to the cyclic structure, which makes the structure more reactive [40]. The C_1 atom carries the excess negative charge of $-0.20e$, while the C_3 atom has a positive charge of $0.28e$. This local geometry and charge transfer are reminiscent of the properties of the 'intimate valence alternation pair' (IVAP) found in a-Se [27, 41]. A valence alternation pair (VAP) allows a system made of chains to lower its energy. Two chains would have four terminal atoms (C_1), which are energetically costly. Combining two chains into a branched structure creates a three-coordinated atom (C_3), reduces the number of C_1 atoms from four to three, and

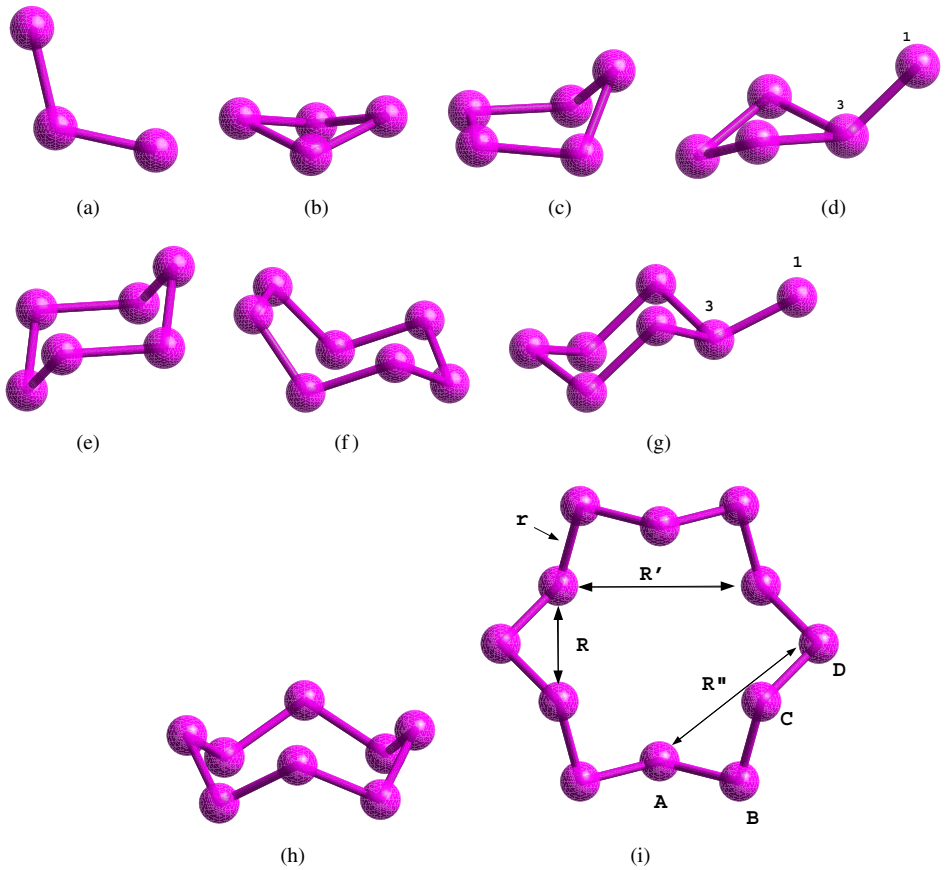

Figure 1. Ball-and-stick models of various Se free-space clusters determined by energy minimization. (a) Se_3, (b) Se_4, (c) Se_5, (d) a higher-energy Se_5 structure, (e) Se_6, (f) the lowest-energy Se_7 structure, (g) a higher-energy Se_7 structure, (h) the Se_8 D_{4d} crown ring, (i) Se_{12} D_{3d}.

thus lowers the total energy of the system. If C_1 and C_3 become nearest neighbours, an IVAP is said to form.

We find for the Se_6 cluster that a D_{3d} ring (shown in figure 1(e)) is the most stable configuration with a Se–Se–Se bond angle of 103°, and a bond length of 2.32 Å in good agreement with the findings of Hohl *et al* [30]. The HOMO–LUMO gap is quite high at 3.6 eV.

Two structures of Se_7 were considered. As for Se_5, the lowest-energy structure is cyclic, and this is shown in figure 1(f). The two torsion angles are 72° and 67°. The structure is similar to the chair structure reported by Hohl *et al* [30]. The bond angles are about 106°, and the bond lengths range from 2.335 Å to 2.76 Å. The HOMO–LUMO gap is 3.31 eV. We have found another dynamically stable Se_7 structure (figure 1(g)), which is 0.99 eV higher in energy than the cyclic structure. The bond lengths in the Se_6 fragment of the structure are very similar to that in the Se_6 cluster. The torsion angles are 68° and 77°. The bond length between the C_1 atom and the C_3 atom is 2.188 Å, similar to that of a dimer. The HOMO–LUMO gap is 2.22 eV which is 1.1 eV smaller than that of the cyclic structure. The terminal C_1 atom carries the excess negative charge of $-0.23e$, while the C_3 atom has a positive charge of $0.25e$. This IVAP defect is similar to that found for C_3–C_1 in the Se_5 cluster.

For the Se_8 cluster, we find a D_{4d} crown ring (figure 1(h)) with a Se–Se–Se angle of 108°, and a bond length of 2.31 Å, in good agreement with the results of Hohl *et al* [30]. The HOMO–LUMO gap is 3.56 eV, which is very close to that of the Se_6 cluster.

The Se_{12} cluster was suggested by Poborchii *et al* [9] to form inside the large cavity of zeolite LTA. The proposed structure is similar to that of the cyclo-dodecasulphur S_{12} and has D_{3d} symmetry (figure 1(i)). The structure found by our first-principles MD optimization is compared with that obtained by Poborchii *et al* with the use of a force-field method in table 2. The HOMO–LUMO gap is 3.58 eV, which is surprisingly close to those of the Se_8 and Se_6.

Table 2. The structure of the Se_{12} D_{3d} cyclic molecule.

Parameter	This work	Poborchii *et al* [9]
r (Å)	2.313	2.32
θ	108°	106°
R (Å)	3.748	3.76
R' (Å)	4.778	4.62
R'' (Å)	4.823	4.744

The Se_{12} molecule is so large that it probably has many low-symmetry isomers. We have considered several cyclic structures, and two types of open chain. An example of a cyclic structure is shown in figure 2(a), and an example of an open chain is shown in figure 2(b). A low-energy cyclic structure (table 1, cyclic Se_{12}) shown in figure 2(a) has an energy 0.34 eV above that of the ground-state cyclic D_{3d} cluster. The bond lengths range from 2.28 Å to 2.38 Å, and the bond angles range from 94° to 108°. The HOMO–LUMO gap is 2.6 eV. A short open chain (table 1, short-chain Se_{12}) is shown in figure 2(b), and is 2.66 eV higher in energy than the D_{3d} cluster, and has only a small gap of 0.155 eV. The bond lengths are near 2.32 Å, except for those formed by the terminal atoms. These terminal-atom bond lengths are significantly shorter (2.2 Å) and are similar to those of the Se dimer. The terminal atoms carry an excess charge of about $-0.14e$, which is about a half of the charge of the C1 atom in the IVAP defect pair. For comparison, a longer (stretched) open chain (table 1, long-chain Se_{12}) was also considered, and it was found to be 0.33 eV higher in energy than the compact shorter chain. The bond lengths and bond angles are similar to those of the compact chain. A difference occurs in the electronic structure since we find complete closure of the HOMO–LUMO gap for the longer chain. This is due to the orbital degeneracy of the dangling bonds on the terminal atoms. As the chain is stretched, the pair of atoms at each end becomes more like a Se dimer. Thus we conclude that for short isolated chains, it is energetically favourable to coil and form a slightly more compact structure. In addition, the reactivity of the more compact chain decreases due to the gap opening.

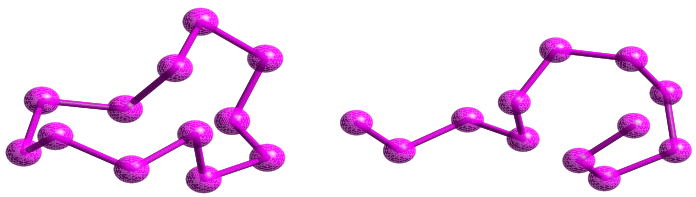

(a) (b)

Figure 2. Some alternative Se_{12} clusters: (a) a cyclic structure; and (b) an open chain structure. Both of these are higher in energy than the ground-state Se_{12} cyclic D_{3d} structure of figure 1(i).

The largest cluster that we consider is Se_{16}. This cluster was suggested to exist inside the zeolite LTA [15]. We consider two possible structures: a double Se_8 ring (D8R); and a cyclic high-symmetry D_{4d} ring. The double Se_8 ring is a parallel stacking configuration of two Se_8 rings, at a distance of 3.89 Å. We find that the energy of this configuration is actually slightly higher than that for two infinitely separated Se_8 rings. However, small van der Waals interactions are not well reproduced with the LDA used here, and these interactions probably stabilize this pair more than is indicated by the calculation performed here. Also we find that the HOMO–LUMO gap is reduced to 2.98 eV, a reduction of nearly 0.6 eV from that for the isolated Se_8 ring. We also considered a cyclic high-symmetry D_{4d} ring. The energy for this ring is very close to that of the S_{16} D8R, and is just 0.07 eV higher than the energy of two non-interacting S_8 clusters. The HOMO–LUMO gap of the D_{4d} ring is 3.28 eV, which is lower than 3.56 eV, the gap of a single Se_8 ring.

The total energies per atom in Se clusters with respect to that of the infinite Se chain are given in table 1. The infinite chain is chosen as a reference energy to illustrate the difference between the two structure types of Se. In particular, this is an important point for amorphous Se, where both rings and chains are believed to be present, but the structure is not known in detail. It is interesting to note that Se_8, Se_{12}, and Se_{16} cyclic molecules are lower in energy than a fully optimized isolated chain. Since Se_8 will be important in our discussion of Se clusters in zeolites, we have investigated the stability of this free cluster and its decomposition into smaller clusters. Se_8 is found to be highly stable with the smallest input of energy required to decompose it into two Se_4 clusters being 2.62 eV.

The HOMO–LUMO gaps are listed in table 1 and an interesting observation is that the low-energy structures of Se_6, Se_8, and Se_{12} all have very similar HOMO–LUMO gaps of about 3.6 eV. This will make them practically indistinguishable in an absorption experiment inside a zeolite cage. We also find that the formation of an even cyclic structure with a 'leg', such as Se_5 and Se_7, closes the gap for the structure by about 1 eV, and results in the formation of an IVAP defect. These defects in condensed phases have been suggested to be responsible for the photosensitivity of Se. Theoretically, they have been considered by Vanderbilt and Joannopoulos [41], and more recently by Zhang and Drabold [27]. We have estimated the energy cost of creating a C_3–C_1 defect pair in a cyclic cluster. To do so we compared the energy of an odd-membered cyclic cluster (e.g. Se_{17}) with a high-symmetry ring with a 'leg' (e.g. Se_{16} + 1). In Se_5, Se_7, Se_9, Se_{13}, and Se_{17} we find the energy cost of creating the C_3–C_1 IVAP defect to be 1.24, 0.99, 0.84, 0.70, and 0.79 eV, respectively. For comparison, we find the formation energy of the C_3–C_1 pair in an infinite isolated chain to be 0.79 eV.

An important remaining question is that of how the C_3–C_1 IVAP defects could form in an isolated cluster. We have found one possible scenario. In a finite-temperature MD simulation we have observed the decomposition of a cyclic Se_{12} cluster into a Se_5 ring and an open Se_7 chain. When we quench from this 'transition state', a cluster consisting of a Se_6 ring and a 'leg' and a Se_5 ring are formed. Therefore we suggest that IVAP defects may form as a result of the decomposition of large cyclic clusters, into chains which then improperly close on themselves.

3.2. Vibrational modes of clusters

Vibrational spectroscopy is widely used for the analysis of amorphous Se and zeolite-encapsulated Se clusters. It is generally accepted that the spectral region between 200 and 300 cm^{-1} is unsuitable for cluster identification. In bulk trigonal Se, the symmetric bond-stretching frequency is at 237 cm^{-1}, and in α-monoclinic Se the A_1-symmetric bond stretch is at 256 cm^{-1}. In bulk materials, the vibrational bands at 84, 114, and 254 cm^{-1} have been

assigned to the Se_8 cluster and are of particular interest. The so-called boson peak is observed below 100 cm^{-1} in amorphous and vitreous solids. The boson peak found in a-Se is described as being in between that of a low-molecular-weight glass and a polymeric glass [42].

Vibrational frequencies of various Se molecules and chains encapsulated in cages and channels of various zeolites have been recently reported. Goldbach *et al* report vibrational bands at 30, 75, 107, 122, 200, and 260 cm^{-1} in Se-loaded zeolite Y [16]. The modes below 150 cm^{-1} are attributed to the Se_8 cluster. The bands at 200, 240, and 260 cm^{-1} are identified with irregular Se chains. These authors have also reported the formation of Se_2^{1-} in Nd-Y [6]. Poborchii *et al* identified Se_8 and Se_6 clusters in the molecular sieve ALPO-5 [45]. They assigned a band at 104 cm^{-1} to Se_6, and bands at 76, 115, and 268 cm^{-1} to Se_8. Surprisingly, the mode at 76 cm^{-1}, identified as an asymmetric bend, has a lower frequency than a corresponding mode reported in bulk Se at 84 cm^{-1} [43]. Poborchii *et al* have also investigated Se clusters in mordenite [44, 46]. They report chain-like vibrations at 256 cm^{-1}, and several cluster-like modes. Bands at 104, 135, and 274 cm^{-1} are attributed to Se_6 clusters, while those at 268 cm^{-1} and 75 cm^{-1} are attributed to Se_8. Most recently Poborchii *et al* have investigated Se clusters in zeolites X and A. It is suggested that Se_{12} rings with the structure of cyclo-dodecasulphur are observed. The bands at 56, 88, and 258 cm^{-1} are attributed to this molecule.

We have investigated the vibrational properties of several Se clusters. The dynamical matrix is computed by displacing each atom of the molecule (or unit cell for solids), in turn, in three orthogonal directions. The force on every atom is evaluated for each displacement, which determines a single row of the force constant matrix by dividing each force by the magnitude of the displacement. The force constant matrix is computed for both positive and negative displacements and averaged to eliminate third-order anharmonicity.

We will first discuss the (Se_2) dimer. Experimentally, for the neutral dimer the frequency of the stretch mode is 385 cm^{-1} [10], while for the charged dimer, Se_2^{1-}, the frequency is only 328 cm^{-1} [6]. Therefore a softening of 57 cm^{-1} of the stretched mode upon charging is observed. We have calculated the stretch frequency for the neutral dimer and obtained 432.6 cm^{-1}. This calculation reproduces the experimental value within 12%. Next, we compute the frequency of the stretch mode for Se_2^{1-} and obtain 377.6 cm^{-1}. Thus we find theoretically a softening of 55 cm^{-1} for the stretch mode, in excellent agreement with experiment (within 4%).

The vibrational frequencies computed for the free Se_3, Se_4, Se_6, Se_8, and Se_{12} clusters are listed in table 3. For the Se_6 cluster the non-degenerate modes at 121, 150, and 274 cm^{-1} seem

Table 3. The theoretical vibrational mode frequencies (cm^{-1}) of important Se clusters. Experimental values are given in parentheses. Degeneracies are indicated by ($\times n$).

Cluster	Frequency (cm^{-1})
Se_2	433 (385)
Se_2^-	378 (328)
Se_3	136, 346, 383
Se_4 (cyclic)	62, 120, 298(×2), 306, 315
Se_6 (D_{3d})	75(×2), 88(×2), 121, 150, 274, 287(×2), 289(×2), 292
Se_8 (D_{4d})	33(×2), 73(×2), 90(×2), 103, 118(×2), 119, 277, 282, 283(×2), 284(×2), 291(×2)
Se_{12} (D_{3d})	20(×2), 20(×2), 30, 38, 48, 72, 73, 76, 89(×2), 110(×2), 123, 124(×2), 141, 277(×2), 280(×2), 281(×2), 288, 289(×2), 290

to match those reported by Poborchii *et al* [44,46]. For the Se_8 cluster, the experimental value of the position of the A_1-symmetric stretch mode is 251 cm^{-1} [29], which we calculate to be 282 cm^{-1}. The 277 cm^{-1} vibration is an optical stretch mode, and the 119 cm^{-1} mode is a symmetric bend. Interestingly enough, modes at about 75 cm^{-1} are present in both Se_6 and Se_8 spectra. We have also calculated vibrational modes for the larger odd-membered clusters Se_5, and Se_7. The ring Se_5 cluster exhibits a peculiar very low-frequency torsion mode at 4 cm^{-1}, and a relatively high-frequency 355 cm^{-1} stretch. A 'kite'-like Se_5 cluster lost this 'soft' mode, but exhibits a high-frequency 'tail-stretch' at 374 cm^{-1} which is close to the theoretical value for the position of the stretch mode of a negatively charged Se dimer. For the ring Se_7 structure the lowest-frequency mode is calculated to be at 25 cm^{-1}, and the highest is at 312 cm^{-1}. The 'tail-stretch' mode for the 'kite'-like Se_7 cluster is found at 360 cm^{-1}. Overall, we observe the modes of these odd-membered clusters to spread over a larger frequency range than those of the even-membered high-symmetry clusters of comparable sizes.

3.3. Crystalline Se

We consider two crystalline forms of Se, α-monoclinic and grey Se. Calculations are performed at the experimental lattice parameters. We did not optimize the lattice parameters because the weak interchain and intermolecular van der Waals-like interactions are not expected to be described properly within the LDA. The GGA has been shown to improve the lattice parameters for Se and Te by adding isotropic pressure to the system [31]. The local bonding is however well described within the LDA.

Grey or metallic Se is the most stable form of Se. It crystallizes in a trigonal structure D_3^4 or D_3^6, and consists of helical chains [32]. There are three atoms in the unit cell; in $P3_121$ (D_3^6, No 152 in the *International Tables for X-Ray Crystallography* [37]) the atoms are at the position 3a ($x0\frac{1}{3}$, $0x\frac{2}{3}$, $\bar{x}\bar{x}0$ with $x = 0.27$).

We have minimized the internal coordinates of grey Se at the experimental cell parameters ($a = 4.35$ Å, $c = 4.96$ Å). The minimized structure is shown in figure 3. The nearest-neighbour Se–Se distance d_1 and the interchain Se–Se distance d_2 are found to be 2.34 Å and 3.47 Å, respectively. The ratio d_1/d_2 is 1.48 which is very close to the experimental value 1.49. It is interesting to note that the second-nearest-neighbour distance along the chain is 3.72 Å which is about 7% longer than d_2. The band structure of grey Se is shown in figure 4. We find an indirect gap of 1.79 eV from L to A. A plane-wave calculation performed with CASTEP [38] (we use the cut-off of 300 eV and an ultrasoft Se pseudopotential) gives a fundamental gap of 0.91 eV from L to H, and a gap of 1.11 eV from L to A. There are only minor differences in valence band between the two calculations.

We have calculated the vibrational modes of grey Se at the Γ point. We have used 64 special k-points to determine the electronic band energies in this calculation. We find a singly degenerate mode at 93 cm^{-1}, doubly degenerate modes at 140 cm^{-1} and at 256 cm^{-1}, and a singly degenerate mode at 258 cm^{-1} corresponding to the symmetric stretch of the chain. This should be compared with the symmetric stretch of a similar isolated chain that we compute at 298 cm^{-1}. The experimental value for the symmetric stretch in grey Se is 237 cm^{-1}. The agreement with experiment is better than 10%.

There are two red monoclinic varieties of Se, α- and β-monoclinic. First observed experimentally by Muthmann in 1890, both structures were refined by Burbank [33, 34]. Burbank concluded that α-monoclinic Se contains Se_8 rings with the point-group symmetry $\bar{8}2m$, while β-monoclinic Se consists of eight-membered chains (rings with one link broken). The broken ring structure of β-monoclinic Se was incorrect, and Marsh *et al* showed that it was an 8-ring-based structure similar to that of α-monoclinic Se [35].

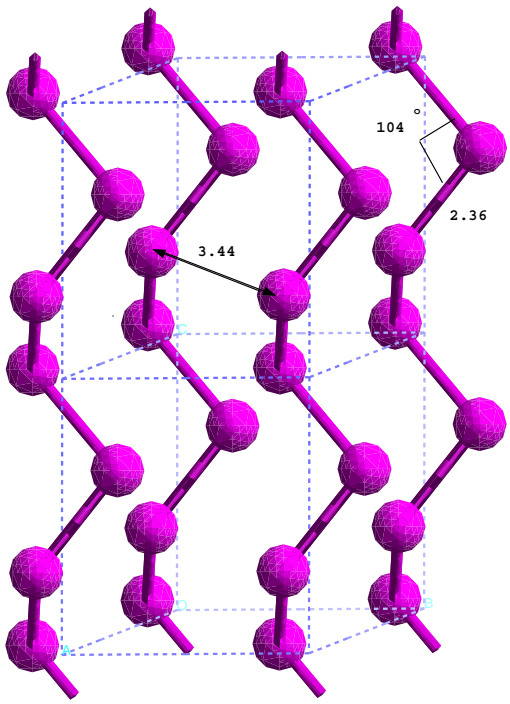

Figure 3. The structure of trigonal Se ($P3_121$ symmetry). The intrachain nearest-neighbour distance is 2.36 Å, while the interchain Se–Se distance is 3.47 Å.

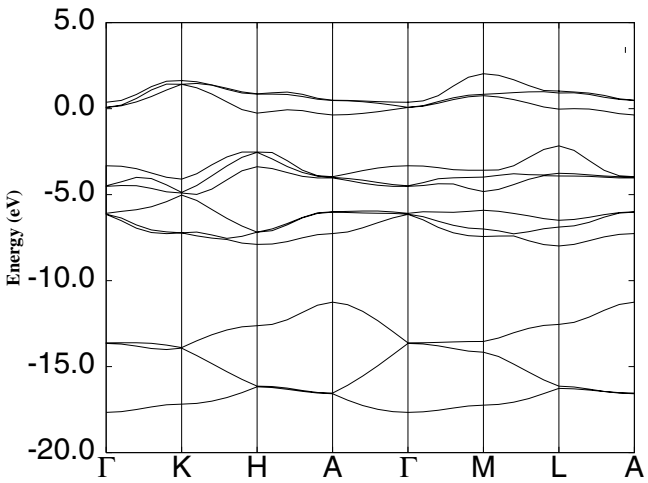

Figure 4. The band structure of trigonal Se. The gap of 1.79 eV is indirect from L to A,

We consider only α-monoclinic Se. There are four Se_8 molecules in the unit cell; the space group is $P12_1/n1$. We use the more recent crystallographic data of Cherin and Ungery [36]. We show in table 4 the lattice parameters and internal coordinates. Calculations were performed using the experimental structure shown in figure 5. The covalent bond distances within the ring are about 2.34 Å and the angles range between 101° and 109°, which can be compared

Table 4. The structure of α-monoclinic Se (from reference [36]). Space group $P2_1/n$, $a = 9.054$ Å, $b = 9.083$ Å, $c = 11.601$ Å, $\alpha = 90.0°$, $\beta = 90.8°$, $\gamma = 90.0°$.

Atom	Position	x, y, z
Se1	4f	0.3209, 0.4840, 0.2362
Se2	4f	0.4254, 0.6625, 0.3569
Se3	4f	0.3178, 0.6376, 0.5378
Se4	4f	0.1343, 0.8186, 0.5529
Se5	4f	−0.0862, 0.6904, 0.5203
Se6	4f	−0.1565, 0.7322, 0.3294
Se7	4f	−0.0814, 0.5217, 0.2290
Se8	4f	0.1301, 0.5990, 0.1337

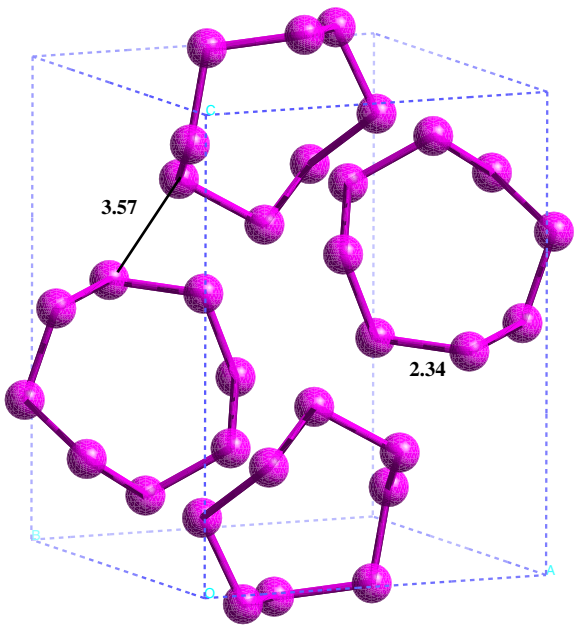

Figure 5. The structure of α-monoclinic Se ($P12_1/n1$ symmetry). The bond distance in the Se_8 ring is 2.34 Å, while the distance between the rings is 3.57 Å.

with 2.36 Å and 105° for grey Se (trigonal). We performed a band-structure calculation, and the dispersion curves are shown in figure 6. We used a tetragonal setting since the monoclinic distortion is very small. The 2.678 eV gap is indirect, as the top of the valence band is along the direction from Γ to X, and the bottom of the conduction band is at R. The gap is reduced by 0.9 eV compared to the HOMO–LUMO gap of a free Se_8 cluster due to the level broadening of the solid.

4. Supralattices: Se in zeolite LTA

4.1. Zeolite Linde type A

Zeolite Linde type A (LTA) is a synthetic aluminosilicate first reported by Breck and co-workers [48, 49], and is built of sodalite β-cages connected through square double 4-rings

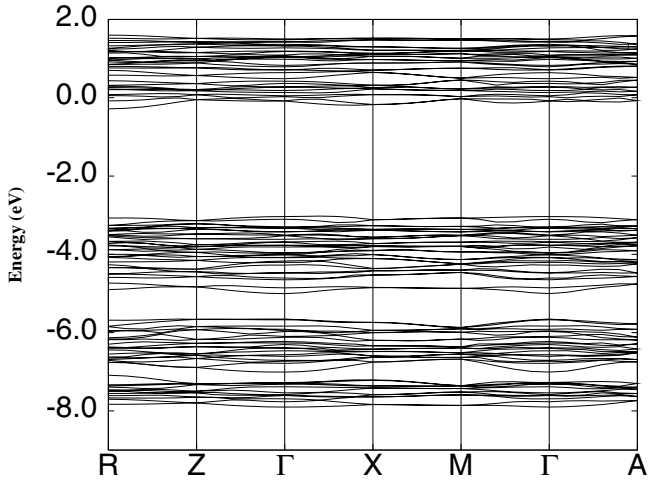

Figure 6. The band structure of α-monoclinic Se. The indirect band gap is 2.678 eV (reduced from the 3.56 eV HOMO–LUMO gap of the isolated Se_8 cluster). The top of the valence band is along the Γ-to-X direction, and the bottom of the conduction band is at R.

(D4R). The voids generated produce the larger α-cages which involve 48 T atoms. The structure contains double 4-rings, and 8-rings. Channels formed by the 8-rings run along the three equivalent ⟨100⟩ directions. The LTA structure is shown in figure 7. LTA is widely used in detergents as a water softener.

Here we consider the all-silica version of type-A zeolite in the idealized structure with space group $Pm\bar{3}m$. We do this for simplicity, since inclusion of aluminium would require us to consider non-framework cations, e.g. Na, and would make the problem less tractable. Since there are no experimental data on the all-silica LTA, we use the aluminated structure of Gramlich and Meier [51] as a starting point. The structural parameters are given in table 5. There are 72 atoms in the unit cell.

Table 5. The structural parameters of the all-silica zeolite A based on the structure from Gramlich and Meier [51]. Space group $Pm\bar{3}m$ (No 221), $a = 12.305$ Å.

Atom	Site	Position
24 Si	24k	0, 0.1847, 0.3694
12 O1	12h	0, 0.2232, 0.5
12 O2	12i	0, 0.2939, 0.2939
24 O3	24m	0.1166, 0.1166, 0.3408

Experimentally, Se clusters are incorporated into voids of the aluminated framework of LTA. Aluminated LTA has a variable lattice constant which depends on the guest (exchangeable cations or molecules) and ranges from 24.84 Å to 23.92 Å [52]. Note that a lattice constant of 24.61 Å (that of Gramlich and Meier) translates into half that (12.305 Å) when we substitute for Al with Si, and we are then able to change from space group $Fm\bar{3}c$ to the primitive space group $Pm\bar{3}m$ [51]. We wish to keep the volume of the cage similar to that of the aluminated crystal, yet do calculations with an all-silica zeolite for simplicity. To understand the relation between the two groups it is easier to start with the $Pm\bar{3}m$ all-silica structure (see table 5). There are 8-rings (formed by T atoms at 24k and oxygens at 12h, 12i) located on each face of the cube, with two T atoms on a line parallel to the cube's edge. The 8-rings on the faces of

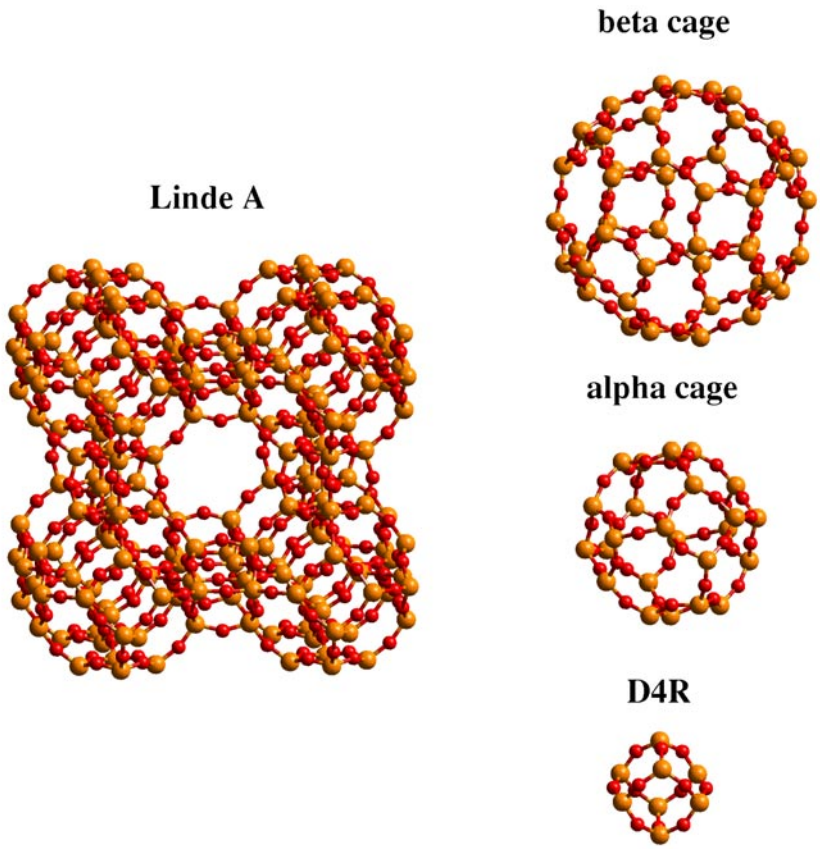

Figure 7. The structure of the all-silica zeolite LTA ($Pm\bar{3}m$ symmetry). There are 24 Si (light grey balls) and 48 oxygen (dark grey) atoms in the unit cell. The structure is built of sodalite β-cages connected by double 4-rings (D4R). The voids thus generated are large α-cages.

two adjacent cells are connected via T–O3–T bridges across the cell edges. The O3 oxygens at 24m sites belong to the LTA's D4R unit, and the T atom is on the face normal to the two under consideration. Substituting for half of the Si T atoms with Al, one has to follow the Löwenstein rule and alternate the metals. This is easy to achieve along a single ring; however, one immediately discovers that, following this strategy, rings in the faces of two adjacent cells become inequivalent. This is the doubling of the cell mentioned above. An fcc translation along the diagonal of the face of this doubled cell becomes the new primitive translation, and we complete our transformation to $Fm\bar{3}c$.

In view of these considerations, we choose the cubic lattice constant $a = 11.8$ Å (space group $Pm\bar{3}m$) since this gives a realistic Si–O bond distance of about 1.6 Å, which is typical of silica polymorphs. Using this cubic lattice parameter, we apply molecular dynamics with a damping force to optimize the internal coordinates of the structure. Our results for the structural parameters are given in table 6. The interatomic distances and angles that we obtain are given in table 7, and are compared with the structural refinements of Gramlich and Meier [51] and Broussard and Shoemaker [50]. The self-consistent charges (Löwdin charges) are computed to be $Q(\mathrm{Si}) = +1.2205e$, $Q(\mathrm{O1}) = -0.614e$, $Q(\mathrm{O2}) = -0.575e$, and $Q(\mathrm{O3}) = -0.626e$. Note that the shortest bond length corresponds to the largest charge transfer. In general, the

Table 6. The structural parameters of the all-silica zeolite A computed with Fireball96. Space group $Pm\bar{3}m$ (No 221), $a = 11.8$ Å.

Atom	Site	Position
24 Si	24k	0, 0.1815, 0.3704
12 O1	12h	0, 0.2270, 0.5
12 O2	12i	0, 0.2930, 0.2930
24 O3	24m	0.1090, 0.1090, 0.3447

Table 7. Bond lengths and angles computed for all-silica zeolite A with Fireball96 ($Pm\bar{3}m$, $a = 11.8$ Å), and compared with experiment.

	θ	$d_{\mathrm{Si-O}}$ (Å)
Si–O1–Si	148.4°	1.586
Si–O2–Si	160.0°	1.600
Si–O3–Si	149.1°	1.573
Experiment: Gramlich and Meier [51]:		
Si–O1–Si	145.5°	1.614
Si–O2–Si	159.5°	1.597
Si–O3–Si	144.1°	1.612
Experiment: Broussard and Shoemaker [50]:		
Si–O1–Si	—	1.660
Si–O2–Si	—	1.670
Si–O3–Si	—	1.670

agreement with experiment is good. Note that the Si–O2–Si angle is the largest, and is in agreement with the experiment of Gramlich and Meier [51]. However, the largest angle does not correspond to the shortest Si–O bond length, which indicates that the lattice constant is not optimized [17]. Experimentally, the T–O2–T angle is larger than the T–O1–T angle for zeolite A with the lattice constant greater than 12.3 Å, which is regarded as a crossover value and indicates the region of the 'soft framework' [52]. This means that for a fixed unit-cell constant, the eight-member rings can easily deform locally. Both oxygen atoms O1 and O2 are located around these rings in twelvefold positions on a twofold symmetry axes, and form a couple of antirotating hinges. The changes in angle around them compensate each other, leaving the overall size of the 12-ring unchanged. It is the oxygen atom O3 located on the D4R unit that is responsible for the overall volume change of the cell (e.g. for the thermal expansion).

We have performed a band-structure calculation for LTA with no Se or other guests in it. The dispersion curves are shown in figure 8. The 10.17 eV direct (Γ-to-Γ) band gap makes it a wide-band-gap insulator. Our method typically overestimates band gaps in silicas due to the use of a minimal sp^3 basis. For comparison, in α-quartz we obtain a band gap of 16 eV, and for melanophlogite a gap of 14.3 eV [17]. These two features, i.e. large regular cages and a wide band gap (which causes optical transparency), identify zeolite A as an ideal host crystal for optical supralattices.

We have also computed the vibrational density of states for Γ-point ($\vec{k} = (000)$) phonons. Phonons at this wavevector are those relevant to Raman or IR experiments. The Γ-point phonon density of states is shown in figure 9. This has been calculated for a cubic cell with the lattice

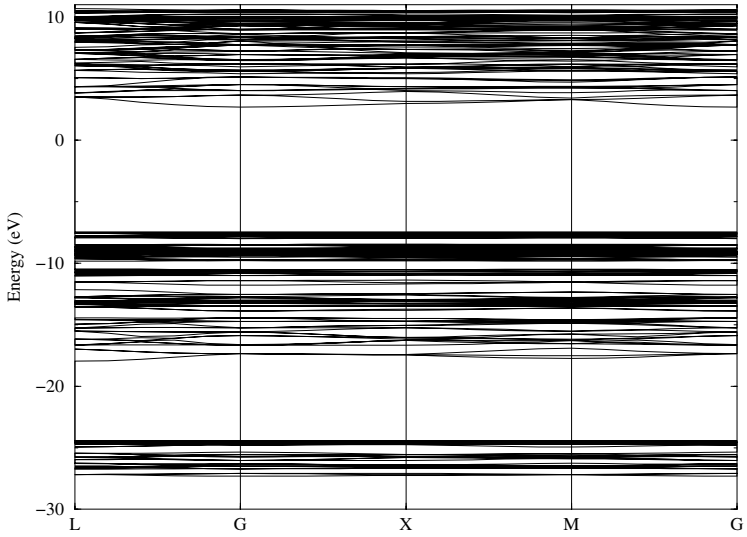

Figure 8. The band structure of the all-silica version of zeolite A. The top of the valence band is near −8.0 eV. A wide band gap (10.17 eV) is found.

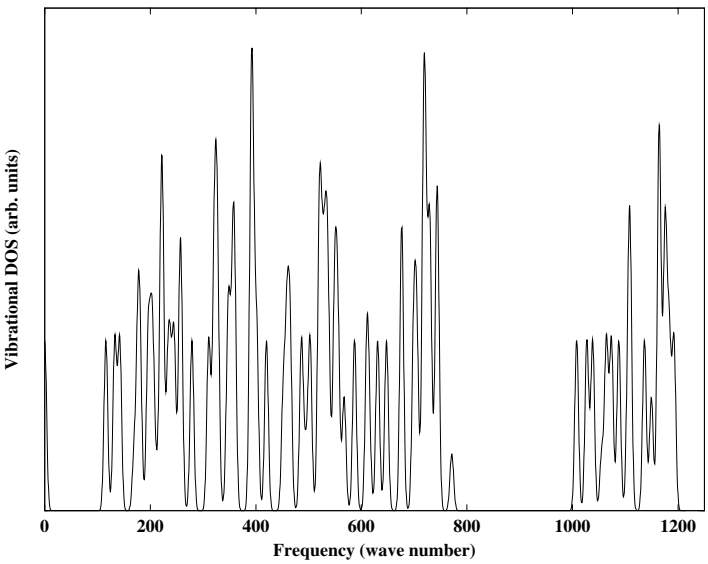

Figure 9. The Γ-point phonon density of states (broadened δ-functions) of the all-silica zeolite A.

constant of 12.0 Å. The important observation is that there are no zone-centre modes below 116 cm^{-1}, which makes this spectral range ideal for the identification of zeolite-encapsulated clusters by means of vibrational optical spectroscopy.

4.2. Optical absorption spectra of Se rings in LTA

Se clusters in zeolites have been studied for the past 20 years. The pioneering work was done by Bogomolov and his group in Leningrad [4, 7]. It is generally accepted that isolated Se

clusters form in zeolite A, while strongly interacting clusters form in zeolites X and Y. On the other hand, Se chains have been observed in channelled zeolites such as mordenite [8, 9], and cancrinite [10]. When zeolite A is exposed to Se vapour, it is believed that isolated ring-like Se clusters form in the supercages (α-cages) of the zeolite. The exact size of these clusters is yet to be determined. In early work, Bogomolov *et al* estimated the number of Se atoms to be about 18 per cage [7]. Later Nozue *et al* [15] lowered that number to 16 (this was partially based on an analogy with sulphur [11]) which suggests a double 8-ring. The most recent interpretation by Poborchii *et al* suggests that the clusters are 12-membered rings structurally similar to the cyclo-dodecasulphur molecule [9]. The optical absorption spectra of Se clusters in zeolite A were measured by Parise *et al* [14] who interpreted a 3.6 eV absorption band as being associated with the Se_8 cluster. Peaks at 3.5 eV and 3.0 eV were reported by Nozue *et al* who investigated Se incorporated in Na-A and Mg-A [15]. In addition, Goldbach *et al* reported a 3.6 eV band and a 3.0 eV band in Sr-Y loaded with Se [16], and more recently Poborchii *et al* reported the same peaks for Se in zeolite A [9]. Summarizing the experimental results, one concludes that there are two peaks in the optical absorption spectrum of Se-loaded caged zeolites: one around 3.0 eV, and one slightly above 3.5 eV. To decipher the origin of these peaks we have performed total-energy and band-structure calculations for Se_8, Se_{12}, and Se_{16}, which we now describe.

First we consider a Se_8 ring in the supercage. We have performed a simultaneous molecular dynamics structural relaxation of the incorporated cluster and of the host zeolite crystal. The final geometry of the cluster located in the middle of the supercage is nearly identical to that of a free cluster. We have calculated the band structure of the resulting nanocomposite, and the near-gap region is shown in figure 10. The most striking feature of this spectrum is that to a good approximation it is a superposition of the dispersionless molecular levels of the cluster within the band diagram of zeolite A. This is typical for supralattices with physi-encapsulation, where the strength of the interaction between the guest and host is between those of the covalent and van der Waals interactions [12]. The HOMO and the LUMO of Se_8 are shifted upward in energy almost uniformly by 0.73 eV and 0.74 eV, respectively. The shift is due to the electrostatic cage potential, and the molecule is too small to experience the non-uniformity of the potential within the cage. The resulting band gap is 3.55 eV, which is almost identical to that of a free Se_8 ring (3.56 eV). The energy of encapsulation is -0.42 eV/atom, meaning that

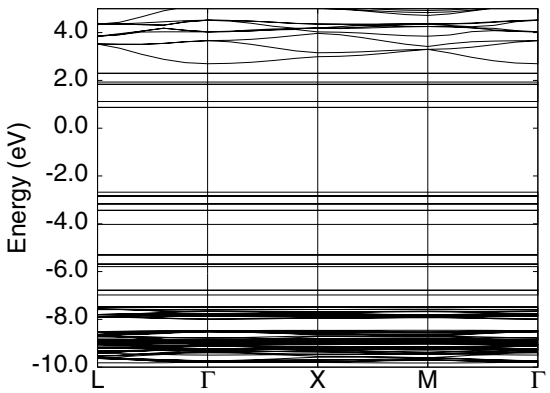

Figure 10. The electronic band structure of a supralattice containing a Se_8 ring in every supercage of the all-silica zeolite A. Only the near-band-gap region is shown. The nearly dispersionless bands in the band-gap region of zeolite A (compare with figure 8) are electronic levels from the Se_8 cluster. The HOMO of the Se_8 cluster is near -2.5 eV.

the energy of the zeolite/Se_8 nanocomposite system is lower than the energy of the separated systems. This encapsulation energy is distributed over many bands (there are over 100 occupied bands), so even the 'Se-derived' bands remain relatively dispersionless.

Next, we consider a sixteen-atom cluster consisting of two parallel eight-membered rings. We relax the cluster and the framework. The encapsulation energy is −0.27 eV/atom, which again indicates that the cluster prefers to be inside the cage. The structure of the cluster, again, has not been significantly affected by encapsulation. The band structure of the resulting nanocomposite is shown in figure 11. The band gap is 2.9 eV, just slightly smaller than the HOMO–LUMO gap of the free cluster (3.0 eV). When compared to the electronic states of free Se_{16}, both the HOMO and the LUMO are shifted upward in energy. However, the HOMO shift of 0.65 eV is larger than that of the LUMO (0.55 eV). We predicted a similar effect theoretically for a five-atom Si cluster in sodalite [12], which was later confirmed experimentally by He *et al* [13]. There are two factors affecting the gap of the encapsulated cluster: the cage 'pressure' and the internal cage potential. Since the structure of encapsulated Se_{16} is practically unchanged in the present case, the closure of the gap upon encapsulation is due mainly to the second effect (the cage potential). The intercage potential is not uniform, and the difference in spatial character of the HOMO and LUMO wavefunctions produces this effect.

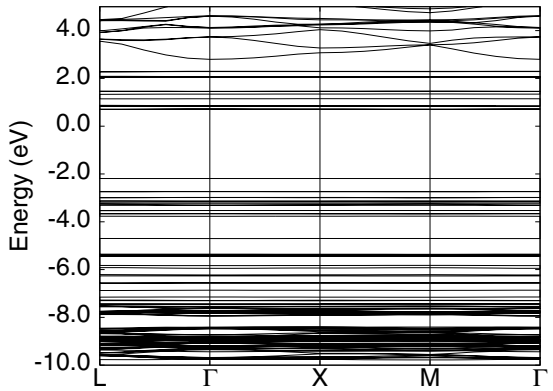

Figure 11. The electronic band structure of a supralattice containing a double 8-ring inside the supercage of all-silica zeolite A. Only the near-band-gap region is shown. The nearly dispersionless electronic states are associated with the cluster. The HOMO of the Se_8 cluster is just below −2 eV.

Finally, we consider a twelve-atom ring cluster inside the α-cage. This structure was recently proposed by Poborchii *et al* [9]. The encapsulation energy is −0.36 eV/atom, indicating that the nanocomposite is indeed stable against the decomposition into a free cluster and zeolite. The band gap of the nanocomposite is 3.49 eV, and the HOMO and the LUMO can be traced to those of a free Se_{12} (HOMO–LUMO gap: 3.59 eV). The structural change due to the encapsulation is rather small; R' has increased from 4.5 Å to 4.6 Å, and the ABC angle θ has reduced from 108° to 106°. Both the HOMO and the LUMO move a few meV upward in energy because of the slight change in the cluster geometry. The cage potential, however, causes a large upward shift of approximately 0.5 eV, where again the HOMO moves up slightly more than the LUMO causing a HOMO–LUMO gap reduction.

To summarize, we have found that Se_8, Se_{12}, and Se_{16} are stable clusters inside the supercage of zeolite A. The encapsulation energy gets smaller (it becomes less energetically favourable) with increase of the cluster size. An estimated rate of energy increase of 0.023 eV/atom indicates that no more than 25 Se atoms can be loaded into the supercage before the Se–framework interaction comes into the picture. This rough estimate agrees well

with a simple geometrical picture. The internal volume of the α-cage is about 730 Å^3, while a Se atom in a condensed phase requires a volume of about 28 Å^3. That establishes an upper limit of 26 atoms per cage.

Our electronic structure calculations suggest that Se_8, Se_{12}, and Se_{16} encapsulated in zeolite A give peaks at 3.6, 3.49, and 2.9 eV, respectively, in the optical absorption spectrum. The HOMO–LUMO gaps of the free clusters are 3.60, 3.56, and 3.28 eV, respectively (see table 1). This shows the trend of a reduction of the HOMO–LUMO gap for larger clusters upon encapsulation. The gap of an encapsulated cluster is affected by two distinct factors—the restricted cage geometry and the non-uniform electrostatic cage potential. The larger the cluster, the more significant the factors. In all three cases studied, both the HOMO and the LUMO move upward in energy, with the HOMO moving by the larger amount, and thus reducing the gap. Such encapsulation-induced reduction of the HOMO–LUMO gap is important to catalytic properties of zeolite-supported clusters, since it increases the reactivity of the encapsulated species [40].

As regards the interpretation of the optical experiments, our calculations suggest that Se_{16} is responsible for the peak observed just below 3.0 eV, while Se_8 and/or Se_{12} is responsible for the peaks above 3.0 eV. It should be added, however, that our calculations give a HOMO–LUMO gap of 3.6 eV for a free Se_6 cluster as well. We do not expect a significant change of this gap upon encapsulation, due to the small size of the cluster. Therefore, rather than lending support to any particular peak assignment in the recent literature, our calculations indicate that the interpretation of the absorption experiments and peak assignments should be treated with extreme caution. The absorption peak itself does not identify the cluster unequivocally, and other experimental techniques must be used to complement the optical data.

4.3. Vibrational spectra of Se rings in LTA

Goldbach *et al* base their identification of the Se_8 in Sr-Y mainly on the Raman data [16]. They reported four Raman-active modes below 150 cm^{-1}, at 30, 75, 107, and 122 cm^{-1}. Poborchii *et al* reported modes at 55, 75, 88, 109, and 135 cm^{-1}, and they attribute them to a twelve-membered cluster with the exception of the 75 cm^{-1} mode, which was assigned to Se_8.

Before we analyse the experimental evidence for particular mode assignments, and compare it with our theoretical results, we would like to consider a fundamental question: to what extent are the vibrational frequencies of a Se cluster affected by encapsulation within a zeolite? We have calculated the vibrational frequencies of the encapsulated Se_8 cluster, and the resulting spectrum is shown in figure 12 (the frequencies are 28, 32, 59, 71, 88($\times$2), 101, 113, 114, 115, 277, 279, 282($\times$2), 283($\times$2), 290, and 291 cm^{-1}). The free-Se-cluster frequencies are listed in table 3, and the vertical lines in figure 12 indicate the frequencies of a free cluster. We see an overall softening of the modes of the encapsulated cluster compared to those of the free cluster. In addition there is a lifting of the degeneracies due to the interactions with the zeolite framework. However, the changes are moderate due to the relatively small size of the cluster. The most significant (and as we will see most important) frequency downshift of 14 cm^{-1} occurred for one of the originally doubly degenerate modes at 73 cm^{-1}. Generally, however, gas-phase vibrational spectroscopy frequencies can be used, if this is done carefully, for encapsulated-cluster identification, provided that the cluster is small enough.

We now analyse the experimental evidence and discuss our theoretical results. At the low-frequency end, we find that a free Se_{12} cluster has a mode at 30 cm^{-1}, and a mode at 38 cm^{-1}. However, the encapsulated Se_8 cluster has similar values for mode frequencies, at 28 cm^{-1} and 31 cm^{-1}. The relative proximity of these modes probably makes them unsuitable for cluster identification. Poborchii *et al* assign the mode at 55 cm^{-1} to Se_{12}. We do not

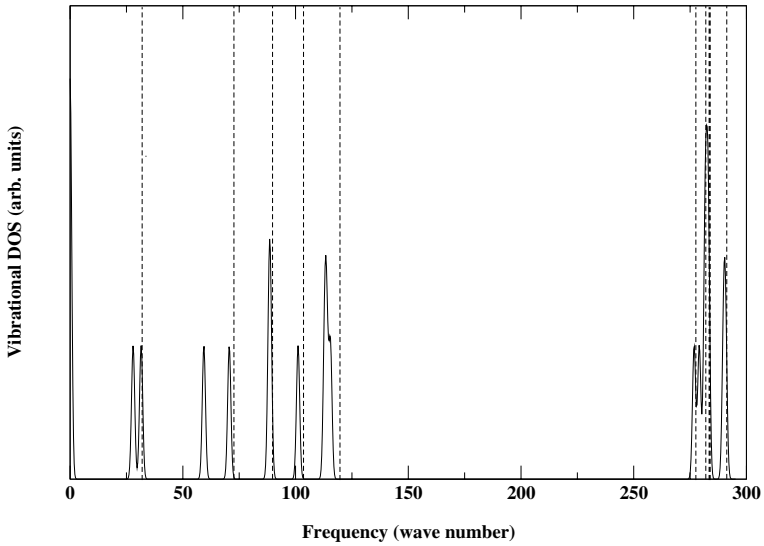

Figure 12. Vibrational spectra of a Se_8 cluster inside the supercage of all-silica zeolite A. The vertical lines show the frequencies of the free-space cluster for comparison. Note that a doubly degenerate mode of a free cluster at 73 cm^{-1} splits upon encapsulation, and a downshifted mode appears at 59 cm^{-1}. This mode is unique to the Se_8 cluster.

see any vibrational modes of this cluster between 48 cm^{-1} and 72 cm^{-1}. Assuming that our frequencies are accurate to within approximately 10%, we conclude that this mode is probably not a signature of Se_{12}. On the other hand, encapsulation of Se_8 splits and shifts the originally doubly degenerate pair of modes at 73 cm^{-1} to produce a mode at 59 cm^{-1} that is close to the one reported by Poborchii *et al*. Thus we interpret the experiments as showing evidence of both Se_8 and Se_{12}. Modes at 88 cm^{-1} and about 110 cm^{-1} are also present in both clusters. However, modes close to 122 cm^{-1} and 135 cm^{-1}, calculated for Se_{12}, are absent in the spectrum of Se_8. Our analysis suggests that both Se_8 and Se_{12} are present in Se-loaded cages of LTA. However, it is also conceivable that the 135 cm^{-1} mode comes from Se_3, while the 122 cm^{-1} mode comes from Se_6 or Se_4 (see table 3). The experimental 55 cm^{-1} mode seems to be a signature mode for encapsulated Se_8 if it can be resolved from the 62 cm^{-1} mode of Se_4.

4.4. Se chains in LTA

Experimentally, Se chains are reported to form in zeolites with well defined channels, e.g. mordenite and cancrinite [8–10]. LTA is rarely viewed as a channelled structure. However, there are clear passages from one α-cage to another. Therefore one can envisage two short open chains in two different cages linking across the 8-ring window separating these cages. We have considered two different chains running along the $\langle 100 \rangle$ direction of LTA. We first investigate a defective irregular chain, and then compare it to a chain similar to those found in trigonal selenium (t-Se).

An irregular chain with twelve Se atoms per cage was prepared by putting two short six-membered chain fragments into the cage and using MD with damping to find the ground-state geometry. The structure is shown in figure 13. Surprisingly, the resulting nanocomposite is an insulator with a band gap of about 2.0 eV. The bond lengths along the chain vary around 2.36 Å. A structural defect—a C_1–C_3 valence alternating pair—is found along the chain. The

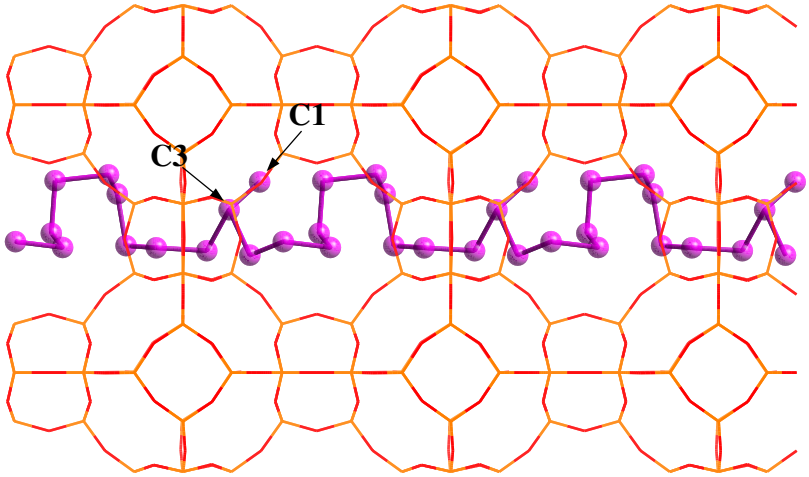

Figure 13. The structure of an irregular Se chain in zeolite LTA with twelve Se atoms per α-cage. The supralattice is insulating with a 2.0 eV gap. There are twelve Se atoms per α-cage. An IVAP defect is stabilized along the chain.

three-coordinated C_3 atom forms two long bonds of 2.39 and 2.46 Å with the chain, and a short 2.21 Å bond with the terminal C1 atom. The C_3 atom has a positive charge of $0.25e$, and the C_1 atom has a negative charge of $0.19e$. This is the first report of such a defect stabilized on a single Se chain.

Next we considered a 'simpler' chain consisting just of seven Se atoms per unit cell. This choice was based on the observation that our lattice constant makes such a chain almost commensurate with the crystal if we take the same pitch as in trigonal selenium. We have minimized the energy of such a chain simultaneously with the host crystal. The resulting geometry is shown in figure 14. A band-structure calculation reveals that the nanocomposite has a band gap of 2.37 eV. For the structure of the embedded chain we find that the bond angles are slightly larger those found in t-Se; the chain appears to be 'stretched'. The bond lengths range from 2.31 to 2.39 Å, and are similar to those in t-Se with the exception of that for the Se–Se pair split by an 8-ring separating the adjacent α-cages, which is significantly shorter (2.26 Å). That is even more surprising given the fact that both Se atoms are slightly positively charged ($Q = 0.024e$). A closer analysis reveals that the Se dimer is trapped by oxygen rings on both sides of the intercage passage (the Se–O distance is 3.2 Å). The charge transfer from Se to O results in a 'charge-density wave' along the chain. A 5.9 Å dipolar domain structure emerges with a 180° domain wall in the middle of the cage. This is to our knowledge the first report of a host-induced ferrielectric transition.

4.5. Se droplets in the α-cages of LTA; a dynamical study

We have performed finite-temperature dynamical simulations of Se_{12} clusters in the α-cages of zeolite A. Simulations have been performed for several picoseconds at various temperatures from 300 K to 2000 K. The state of the system was probed by monitoring the kinetic temperature ($T_{kinetic} = \frac{1}{2}m\langle V^2\rangle/(\frac{3}{2}k)$). We also compute the radial distribution functions from the collected trajectories for Se atoms, and atoms of the host framework as well as Se–framework distributions. A series of RDFs are shown in figures 15(a), 15(b), 15(c) corresponding to 300 K, 1200 K, and 2000 K respectively. One can see that as the temperature rises the peaks

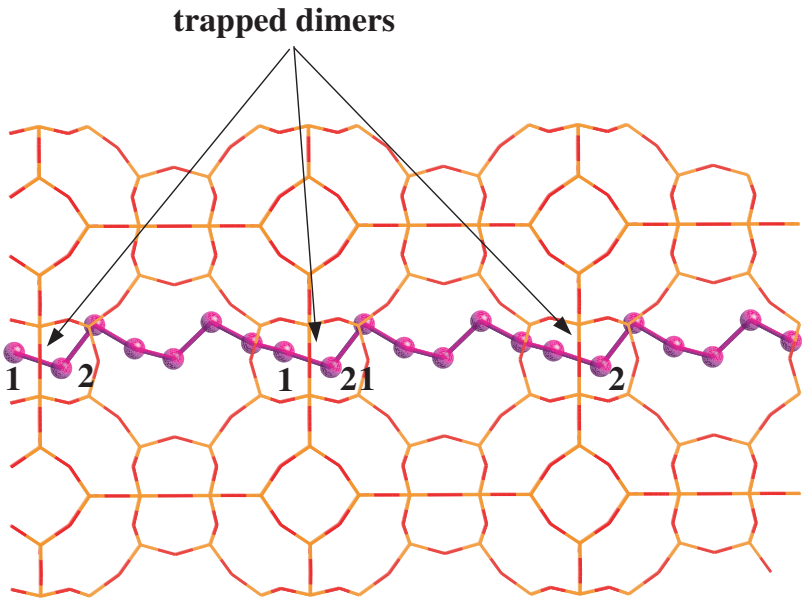

Figure 14. The structure of a Se chain in zeolite LTA. There are seven Se atoms per α-cage. A weak ferrielectric domain structure along the chain is induced by the host crystal.

corresponding to third and fourth neighbours disappear, and the distribution comes to resemble that of liquid Se [53]. The sharp structure at low temperature also becomes 'washed out' at higher temperature. We conclude that at 1200 K we have produced a nanodroplet of liquid Se encapsulated in the α-cage.

An interesting phenomenon is observed in a high-temperature 2000 K run. The Se–Se RDF shows that the cluster is melted and is in a liquid state. However, when we compute the kinetic temperature for just the Se cluster, a sharp drop is revealed after about 6 ps (figure 16); this would indicate a liquid-to-liquid 'phase transition'. To identify this new state of the droplet we obtain the power spectrum from the Fourier transform of the Se-atom velocity autocorrelation function for the first 6 ps, and for the following 6 ps. The power spectra are shown in figure 17. The most striking feature of the spectra is that the later 6 ps portion loses the Se–Se bond-stretch signal at 267 cm^{-1} and it is replaced by a peak at much lower frequency near 150 cm^{-1}. The Se–Se bonds that occur in this later state are more 'dynamic', meaning that the bonds are only temporary. Bonds are being broken and reformed with different atoms at a faster rate, leading to this change in vibrational spectrum. The cluster has taken on the characteristics of a high-density confined nanovapour.

5. Conclusions

In conclusion, we report the first theoretical study of Se-loaded supralattices templated by zeolite A. In addition, comprehensive investigations of various Se clusters and two crystalline polymorphs, as well as the structure and properties of the all-silica form of zeolite A are reported. We find Se_8, Se_{12}, and Se_{16} cyclic clusters to be the most stable clusters. It is found that Se_6, Se_8, and Se_{12} have almost identical HOMO–LUMO gaps of around 3.6 eV. We estimate the formation energy of the intimate valence alternation pair C_3–C_1 (the defect

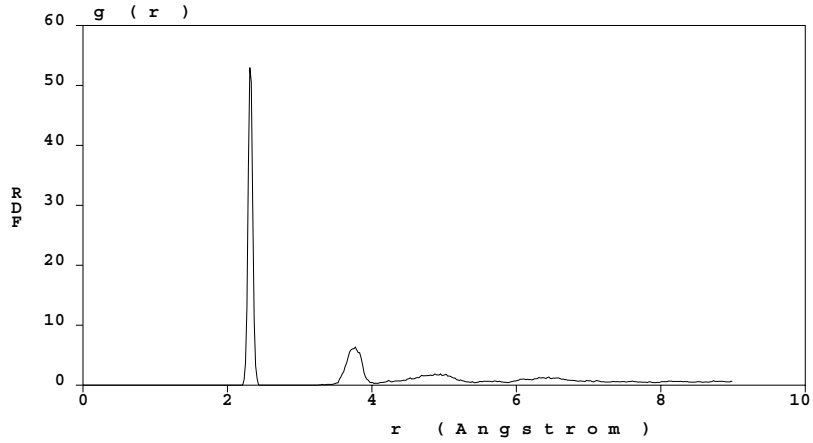

(a)

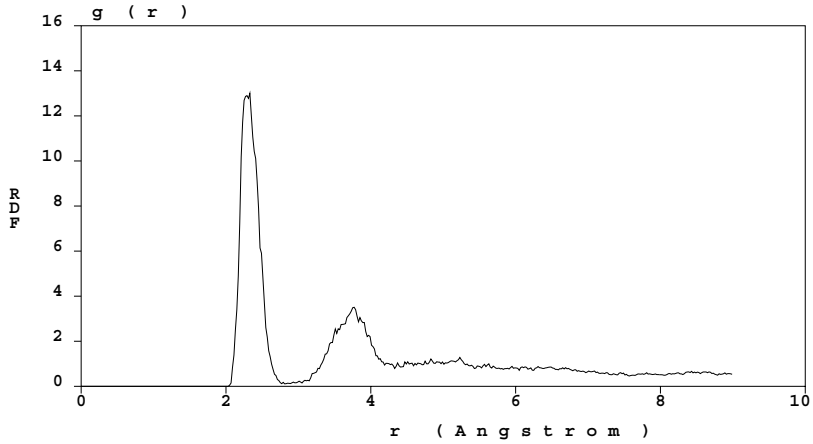

(b)

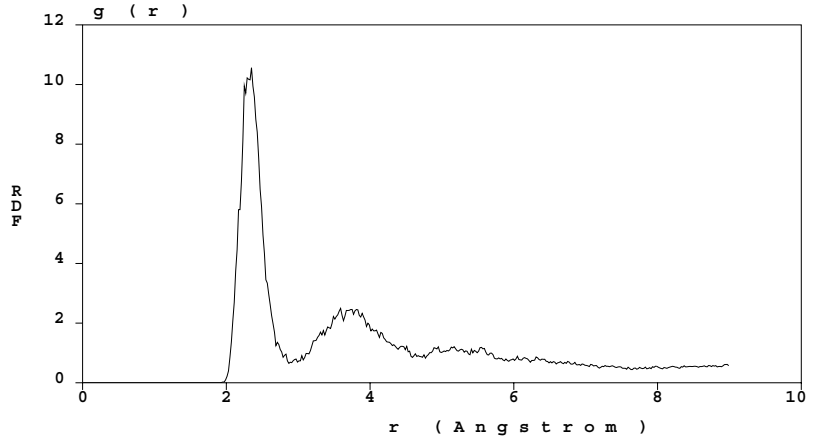

(c)

Figure 15. The Se–Se radial distribution functions at: room temperature (a); 1200 K (b); and 2000 K (c) for the Se_{12} cluster encapsulated in the α-cage of zeolite LTA.

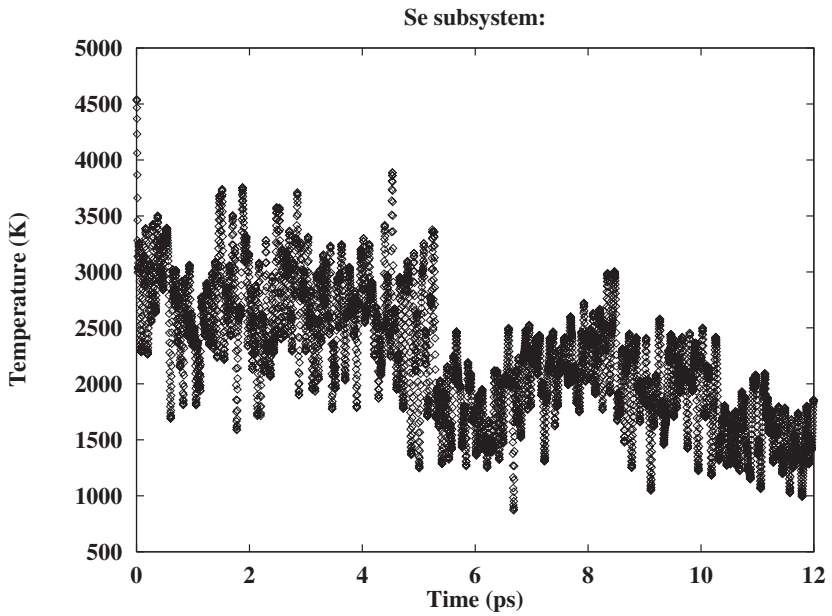

Figure 16. The kinetic temperature computed for the Se_{12} cluster during a 20 ps MD run at the average temperature of 2000 K for the host–guest system.

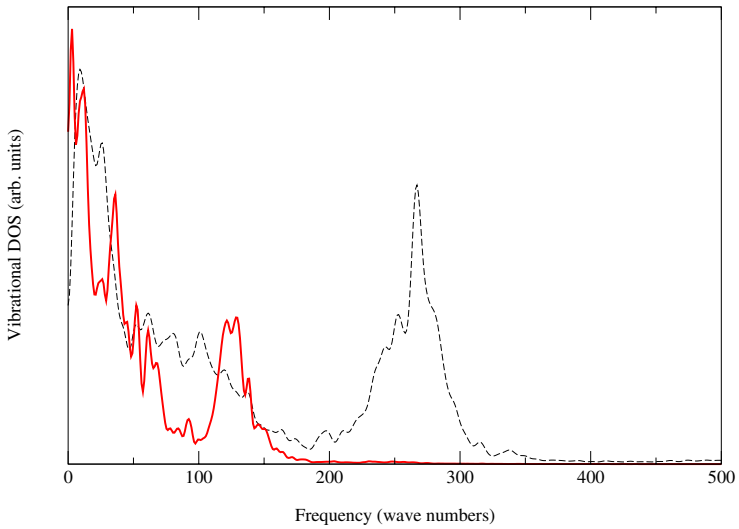

Figure 17. The power spectrum computed for the first 6 ps (dashed line) and the following 14 ps (solid line) of the 2000 K MD run for twelve Se atoms in LTA. Note the disappearance of the Se–Se stretch at 267 cm^{-1} in the later section indicating a new liquid (quasi-vapour) phase of the cluster.

responsible for the photoactivity of Se), and find it slowly diminishing with increasing cluster size. It reaches 0.79 eV for the infinite isolated chain for a cluster as small as 17 Se atoms. Calculated vibrational frequencies are in good (about 10%) agreement with the available experimental data.

Zeolite LTA is found to be an optically transparent insulator. Its vibrational spectrum at the zone centre has a frequency window below 116 cm^{-1} suitable for the identification of the encapsulated Se species. First we consider cyclic-cluster-loaded zeolite A. Using the rate of increase of the encapsulation energy with the cluster size, we estimate that up to 25 Se atoms can be physi-encapsulated in the α-cage, in accordance with a simple geometric argument. Our results suggest that encapsulation may increase the reactivity of the cluster due to the HOMO–LUMO gap reduction found in the confined clusters. The electronic structure calculations suggest that the absorption experiment alone is not enough to provide specific assignments of the peaks to Se_8, Se_{12}, or Se_{16} cyclic clusters. Our analysis of the vibrational spectra suggests that the observed Raman mode at 55 cm^{-1} is a signature of the encapsulated Se_8 cluster, that a mode at 135 cm^{-1} indicates the presence of the Se_{12} cluster, and that encapsulation of both clusters has been observed in recent experiments.

Two chain-based supralattices considered here are found to be insulating. For the first time an IVAP C_3–C_1 defect is found stabilized on a single Se chain. We also report that a dimerization induced in a chain by a D4R intercage passage results in a dipolar domain structure along the encapsulated chain. In a high-temperature molecular dynamics run performed for the encapsulated cyclic Se_{12} cluster, we observe a phase transition resulting in the formation of a confined pseudo-vapour Se droplet.

The main conclusion of this work is that supralattices, i.e. nanocomposites consisting of nanosize clusters regularly suspended in inert host matrixes, exhibit a plethora of new, unexpected, and exciting physical phenomena, many of which have potential applications.

Acknowledgments

We thank Vladimir Poborchii, Tetsuya Kodaira, Marie-Louise Saboungi, Yasuo Nozue, Osamu Terasaki, and David Drabold for many stimulating discussions, preprints, and encouragement. We thank Xiaodong Zhang for a critical reading of the manuscript. AAD thanks Werner Baur for an enlightening introduction to the concept of a flexible but non-collapsible framework, and Ed Hall for his support. OFS thanks the National Science Foundation (NSF DMR 99-86706) for support.

References

[1] Stucky G D and MacDugall J E 1990 *Science* **247** 669
[2] Ozin G A 1992 *Adv. Mater.* **4** 612
[3] Demkov A A and Sankey O F 1996 *Chem. Mater.* **8** 1793
[4] Bogomolov V N, Lutsenko E L, Petranovskii V P and Kholodkevich S V 1976 *JETP Lett.* **23** 483
[5] Katayama Y, Yao M, Ajiro Y, Inui M and Endo H 1989 *J. Phys. Soc. Japan* **58** 1811
[6] Goldbach A, Iton L, Grimsditch M and Saboungi M-L 1996 *J. Am. Chem. Soc.* **118** 2001
[7] Bogomolov V N, Kholodkevich S V, Ramanov S G and Agroskin L S 1983 *Solid State Commun.* **47** 181
[8] Kouchaf L, Tuilier M, Guth J and Elouadi B 1996 *J. Phys. Chem. Solids* **57** 251
[9] Poborchii V V, Ivanova M S, Petranovskii V P, Barankov Yu A, Kasuya A and Nishina Y 1996 *Mater. Sci. Eng.* A **217+218** 129
[10] Poborchii V V 1994 *J. Phys. Chem. Solids* **55** 737
[11] Seff K 1972 *J. Phys. Chem.* **76** 2601
[12] Demkov A A and Sankey O F 1997 *Phys. Rev.* **56** 10 497
[13] He J, Ba Y, Ratcliffe C I, Ripmeester J A, Klug D D, Tse J S and Preston K F 1998 *J. Am. Chem. Soc.* **120** 10 697
[14] Parise J B, McDugall J E, Herron N, Farlee R, Sleight A W, Wang Y, Bein T, Moller K and Moroney L M 1988 *Inorg. Chem.* **27** 221
[15] Nozue Y, Kodaira T, Terasaki O, Yamazaki Y, Goto T, Watanabe D and Thomas J M 1990 *J. Phys.: Condens. Matter* **2** 5209
[16] Goldbach A, Iton L and Saboungi M-L 1996 unpublished

[17] Demkov A A, Ortega J, Sankey O F and Grumbach M P 1995 *Phys. Rev.* B **52** 1618
[18] Ceperley D M and Alder G J 1980 *Phys. Rev. Lett.* **45** 566
Perdew J and Zunger A 1981 *Phys. Rev.* B **23** 5048
[19] Hamann D R, Schlüter M and Chiang C 1979 *Phys. Rev. Lett.* **43** 1494
[20] Harris J 1985 *Phys. Rev.* B **31** 1770
[21] Sankey O F and Niklewski D J 1989 *Phys. Rev.* B **40** 3979
[22] Monkhorst H J and Pack J D 1976 *Phys. Rev.* B **13** 5188
[23] Sankey O F, Demkov A A, Windl W, Fritsch J H, Lewis J P and Fuentes-Cabrera M 1998 *Int. J. Quantum Chem.* **69** 327
[24] Miyamoto Y 1980 *Japan. J. Appl. Phys.* **19** 1813
[25] Becker J, Rademann K and Hensel F 1991 *Z. Phys.* D **19** 233
[26] Hohl D and Jones R O 1991 *Phys. Rev.* B **43** 3856
[27] Zhang X and Drabold D 1998 *J. Non-Cryst. Solids* **241** 195
[28] Joannopoulos J D, Schlüter M and Cohen M L 1975 *Phys. Rev.* B **11** 2186
[29] Martin R M, Lucovsky G and Helliwell K 1976 *Phys. Rev.* B **13** 1383
[30] Hohl D, Jones R O, Car R and Parrinello M 1987 *Chem. Phys. Lett.* **139** 540
[31] Kresse G, Furthmuller J and Hafner J 1994 *Phys. Rev.* B **50** 13 181
[32] Bradley A J 1924 *Phil. Mag.* **48** 477
[33] Burbank R D 1951 *Acta Crystallogr.* **4** 140
[34] Burbank R D 1951 *Acta Crystallogr.* **5** 236
[35] Marsh R E, Pauling L and McCullough J D 1953 *Acta Crystallogr.* **6** 71
[36] Cherin P and Ungery P 1982 *Acta Crystallogr.* B **24** 1968
[37] *International Tables for Crystallography* 1996 ed T Hahn (Dordrecht: Kluwer)
[38] The CASTEP program as implemented in the Cerius2 package distributed by MSI, Incorporated.
[39] Li Z Q, Yu J Z, Ohno K, Gu B L, Czajka R, Kasuya A, Nishina Y and Kawazoe Y 1995 *Phys. Rev.* B **52** 1524
[40] Zicovich-Wilson C M, Corma A and Viruela P 1994 *J. Phys. Chem.* **98** 10 863
[41] Vanderbilt D and Joannopoulos J D 1983 *Phys. Rev.* B **27** 6311
[42] Baganich A A, Mikla V I, Simak D G, Sokolov A P and Shebanin A P 1991 *Phys. Status Solidi* b **166** 297
[43] Steudel R 1975 *Z. Naturf.* a **30** 1481
[44] Poborchii V V 1996 *Chem. Phys. Lett.* **251** 230
[45] Poborchii V V, Kolobov A V, Caro J, Zhuravlev V V and Tanaka K 1997 *Chem. Phys. Lett.* **280** 17
[46] Poborchii V V, Kolobov A V, Oyanagi H, Romanov S G and Tanaka K 1997 *Chem. Phys. Lett.* **280** 10
[47] Poborchii V V 1998 *Solid State Commun.* **107** 513
[48] Breck D W, Eversole W G, Milton R M, Reed T B and Thomas T L 1956 *J. Am. Chem. Soc.* **78** 5963
[49] Reed T B and Breck D W 1956 *J. Am. Chem. Soc.* **78** 5972
[50] Broussard L and Shoemaker D P 1960 *J. Am. Chem. Soc.* **82** 1041
[51] Gramlich V and Meier W M 1971 *Z. Kristallogr.* **133** 134
[52] Baur W H 1992 *J. Solid State Chem.* **97** 243
[53] Edeling M and Freyland W 1981 *Ber. Bunsenges. Phys. Chem.* **85** 1049